Magnetism and structure of chemically disordered $FePt_3$ nanocubes

O. Margeat,* M. Tran,† M. Spasova, and M. Farle
Fachbereich Physik and Center of Nanointegration Duisburg-Essen (CeNiDE), Universität Duisburg-Essen, Lotharstrasse 1, 47048 Duisburg, Germany

(Received 4 January 2007; revised manuscript received 19 February 2007; published 12 April 2007)

We report the chemical synthesis, crystal structure, and magnetic properties of single-crystalline $FePt_3$ nanocubes with a side length of 8 nm and a narrow size distribution. As-prepared cubes are in the fcc chemically disordered phase with {100} crystal facets. Self-assembly of the nanocubes results in square superlattices with the ⟨100⟩ directions oriented perpendicular to the substrate plane. The average magnetic moment of $0.63\mu_B$ per $FePt_3$ formula unit and the Curie temperature (T_C=255 K) of the particles are found to be reduced by 20% and approximately 30% with respect to those of the bulk alloy. The effective magnetic anisotropy energy density $K_{eff}=(6.7\pm1)\times10^4$ J/m^3 at 5 K is found to be larger by at least a factor of 2 with respect to bulk values. The temperature dependence of K_{eff}, which is of single-ion origin, follows the magnetization M according to $K_{eff}\sim M(T)^{2.1}$.

DOI: 10.1103/PhysRevB.75.134410 PACS number(s): 75.50.Tt, 75.30.Gw

I. INTRODUCTION

A big advantage for the manufacturing of magnetic data storage media based on the self-assembly of colloidal particles is the use of hard-magnetic nanocubes.[1–3] The magnetocrystalline anisotropy of alloys of Fe_xPt_{1-x} can vary from zero for x=0.75 to $K_{eff}\sim10^7$ J/m^3 for x=0.5 in the $L1_0$ ordered phase.[4] In Pt rich alloys, it was observed that a preferential Pt segregation to the (111) surface occurs, resulting in an almost pure Pt topmost layer and a monotonically decreasing concentration profile for the second and third layers.[5,6] Similar evidence was also found in FePt nanoparticles prepared in the gas phase,[7] which showed a significant oxidation resistance.[8] The question arises if such a behavior can be exploited to design FePt nanocubes with a Pt shell when starting from a Pt rich alloy such as $FePt_3$. Bulk $FePt_3$ is either ferromagnetic in the chemically disordered state (fcc $A1$) with a Curie temperature of 360–400 K or antiferromagnetic with two coexisting phases [Néel temperatures $T_{N1}\sim160$ K and $T_{N2}\sim120$ K (Ref. 9–11)] in the ordered fcc $L1_2$ structure with an Fe atom at the corners of each cubic cell and a Pt atom in the middle of each face. The Fe magnetic moments ($3.3\mu_B$) order in alternating ferromagnetic sheets either in the (110) planes ($T<160$ K) or in the (100) planes ($T<100$ K). Fe moments of $\mu^{Fe}\sim3.1-3.3\mu_B$, a uniaxial anisotropy $K_2=3.9\times10^4-6\times10^3$ J/m^3, and a Curie temperature $T_C\sim360-400$ K have been reported.[12,13] The average magnetic moment per formula unit $\overline{\mu_{at}}$ of fcc chemically disordered "$Fe_{0.25}Pt_{0.75}$" varies between $\overline{\mu_{at}}$=0.78 and $1.06\pm0.05\mu_B$ for $0.2<x<0.3$.[14] Here, we present a study of the magnetic, compositional, and structural properties of chemically disordered monodisperse $FePt_3$ nanocubes produced by organometallic synthesis.

II. SYNTHESIS

The preparation follows the traditional route for the synthesis of FePt nanoparticles (NPs),[15] and only slight changes were introduced to obtain the cubic shape. Briefly, in an inert atmosphere, platinum (II) acetylacetonate ($Pt(acac)_2$, 197 mg, 0.5 mmol), hexadecylamine (HDA, 966 mg, 4 mmol), and oleic acid (OA, 1280 μl, 4 mmol) were mixed in a Fischer-Porter bottle in the presence of 15 ml *o*-dichlorobenzene as solvent. After stirring for homogenization, iron pentacarbonyl [$Fe(CO)_5$, 65 μl, 0.5 mmol] was added to this yellow solution. The bottle was then heated for 24 h in an oil bath at 170 °C. The black dispersion was subsequently cooled down to room temperature. Precipitation of the NPs was achieved by addition of 40 ml of ethanol. After filtration, a small amount of heptane was added to disperse the particles, and then ethanol was used to precipitate them again (three precipitation steps with heptane and ethanol were done). The final precipitate can be dried under vacuum to obtain the NPs as a black powder (60 mg), or easily dispersed and stored in heptane solution containing a small amount of HDA and OA. As compared to other recently published methods for FePt nanocube synthesis,[2,3] there was no need to slowly increase the temperature to 170 °C. Moreover, the long-chain amine can be added simultaneously with the other reactants at ambient temperature, differing from methods with delayed injection. All synthesis steps were performed in a glovebox under argon atmosphere (less than 0.1 ppm O_2 and H_2O). All the solvents were degassed before use by the freeze-pump-thaw technique.

III. EXPERIMENTAL RESULTS

Samples for structural and compositional investigations by high-resolution transmission electron microscopy (HRTEM) and energy dispersive x-ray[16] (EDX) spectroscopy were prepared by slow evaporation of one drop of the highly diluted suspension of NPs on a standard carbon-coated copper grid. X-ray diffraction was performed on samples prepared on a specially cut "no-background" silicon wafer using Cu $K\alpha$ radiation (λ=0.1542 nm). The composition of the nanocubes was determined by EDX spectroscopy using the TEM nanoprobe mode with a convergent beam for spatially resolved analysis.

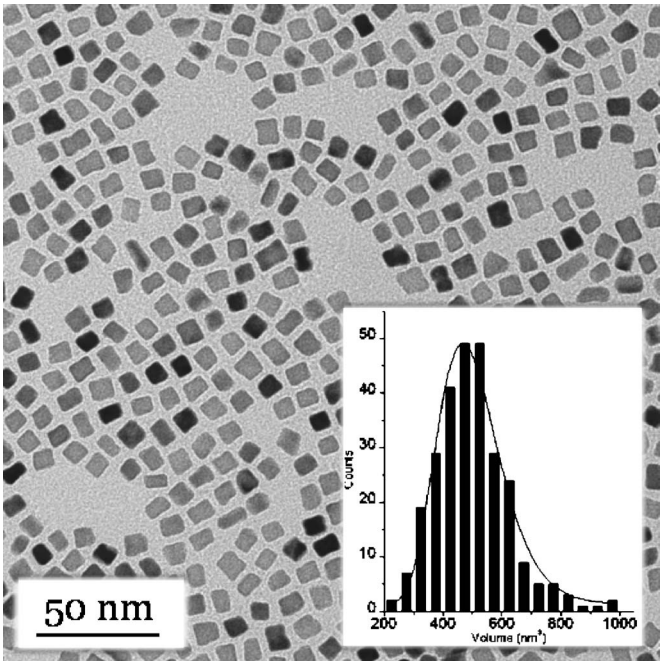

FIG. 1. Bright-field TEM micrograph of the $FePt_3$ nanocubes assembled on a carbon-coated Cu grid. The inset shows the volume histogram of the $FePt_3$ nanocubes determined from the TEM images and the fit according to Eq. (1).

For magnetic measurements in magnetic fields of up to 5 T between 5 and 300 K, the $FePt_3$ nanocube solution was dried under an inert argon atmosphere and weighted (8 mg). The magnetic moment per volume or per nanocube was calculated from the density of $FePt_3$ material neglecting the weight of residual ligands. The accuracy of this approximation is estimated to be better than 10%. For all magnetic data shown below, the background signals from the substrate, residual ligands, and specimen holder, which were measured separately, were subtracted.

A. Shape and crystallographic structure

Figure 1 shows a typical TEM image of the $FePt_3$ nanoparticles. The TEM micrograph indicates that the nanoparticles are of nearly cubic shape with a side length of ~8 nm. Approximately only 3% of the particles deviate from the cubic shape with an aspect ratio larger than 2. The average egde-to-edge distance between neighboring cubes is ~3.5 nm.

The volume histogram determined from the TEM images follows a lognormal distribution

$$f(V) = \frac{1}{\sqrt{2}\pi\sigma_V V} \exp\left(-\frac{\ln^2(V/V_{mp})}{2\sigma_V^2}\right), \qquad (1)$$

with the most probable volume $V_{mp}=490$ nm^3, a standard deviation of ln V of $\sigma_V=0.22$, and an average particle volume $\langle V_p\rangle=502$ nm^3 which is given by $\langle V_p\rangle=\int_0^\infty Vf(V)dV$ and $\langle V_p\rangle=V_{mp}\exp(\sigma_V^2/2)$. The average length of the cube edges is 7.9 nm. The $Fe_{0.25}Pt_{0.75}$ cubes have a tendency to self-assemble in a two-dimensional colloidal crystal with a four-fold symmetry and a volume fraction of the magnetic material of about 39%.

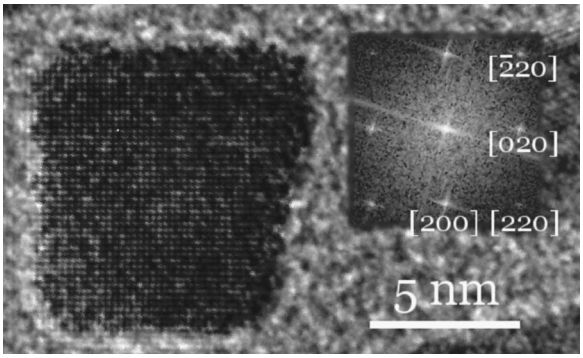

FIG. 2. Typical high-resolution TEM image of an individual $FePt_3$ nanocube. The inset shows the corresponding fast Fourier transform. The electron-beam direction is [001].

The EDX analysis yields a mean composition of $Fe_{29}Pt_{71}$ which is slightly on the Fe rich side and very close to the stoichiometric $FePt_3$ alloy. In order to check the uniformity of the particle composition, spatially resolved EDX studies on more than 30 nanocubes have been performed using the TEM nanoprobe mode with a beam diameter of 10 nm. The composition of individual particles does not deviate from the average value by more than 2.6 at. %. The composition distribution appears to be quite narrow as compared to other Fe_xPt_{1-x} nanoparticles synthesized from the $Fe(CO)_5$ precursor.[17] The composition is also confirmed by the observation of the formation of the $L1_2$ $Fe_{0.25}Pt_{0.75}$ phase after annealing of the sample.

Figure 2 shows a typical HRTEM image of an individual nanocube with very good crystallinity and a quasicubic shape. The cube sides are the {100} crystal planes of the fcc structure. A rounding at the edges, i.e., the formation of small {110} facets of at most five to ten atom columns, is frequently observed. The inset of Fig. 2 displays a fast Fourier transform of the cube image, showing the fourfold symmetry of the fcc structure viewed with the electron beam in the [001] direction. No evidence of superstructure reflexes is observed, indicating that the as-synthesized $FePt_3$ nanocubes are in a chemically disordered fcc ($A1$) phase. This is confirmed by x-ray- and electron-diffraction studies of the nanocube assembly (Fig. 3).

Both diffraction patterns show a set of reflexes typical for the fcc crystal structure. No superlattice reflexes are visible, in agreement with the HRTEM observation of the chemically disordered fcc phase of the $FePt_3$. Analysis of the diffraction patterns yields the lattice parameter $a=0.390\pm0.01$ nm, which is within the error bar, the same as the one of chemically disordered ($A1$) $FePt_3$ bulk [$a=0.387$ nm for $Fe_{30}Pt_{70}$ (Ref. 18)]. A clear [001] texture is evident in the x-ray-diffraction (XRD) pattern as the intensity I_{002} of the (002) peak is higher than the one of (111), which differs significantly from the intensity ratio $I_{111}/I_{200}=5/2$ of a powder spectrum of fcc crystallites. This [001] texture is additionally confirmed by electron diffraction (ED) (inset of Fig. 3, left) as the ⟨200⟩ ring is brighter than the ⟨111⟩ one in the ED pattern. The homogeneity of the ⟨200⟩ ring brightness indi-

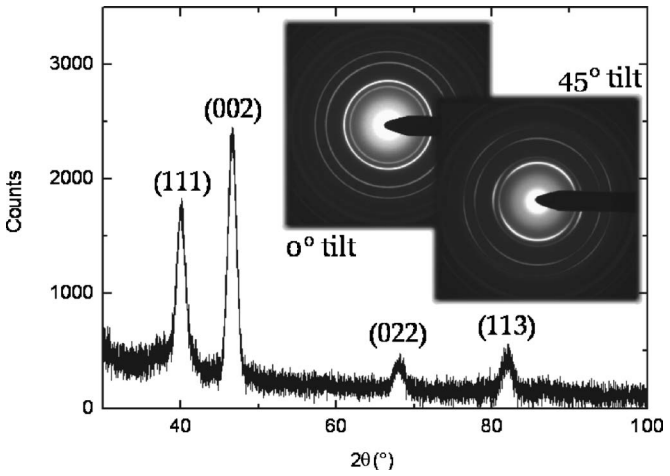

FIG. 3. X-ray- and electron-diffraction patterns of the $FePt_3$ nanocube assembly. Electron-diffraction patterns have been taken with the electron beam perpendicular to the particle layer (0° tilt, left) and after 45° tilting of the sample (45° tilt, right) with respect to the beam.

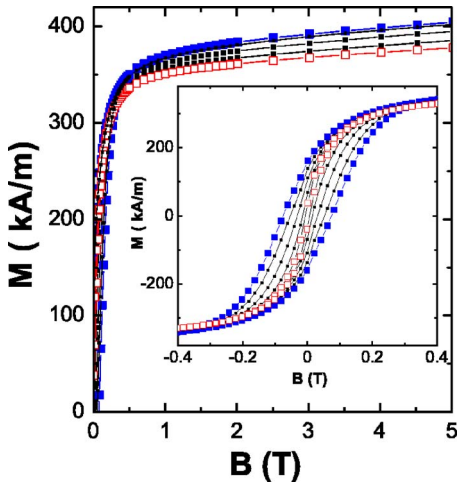

FIG. 4. (Color online) Magnetization isotherms of the $FePt_3$ nanocubes recorded at temperatures 5 K (solid square) and 10, 20, 35, and 50 K (open square). The inset shows details of the hysteresis loops $M(B)$ for ±0.4 T.

cates the absence of long-range in-plane order of the $FePt_3$ nanocubes. The inhomogeneity of the intensity of the diffraction rings, which is observable at a 45° tilt of the sample (inset of Fig. 3, right), is another evidence for a [001] texture of the nanocube assembly.[19]

B. Magnetic properties

In the following, we will show that the assembly of $Fe_{29}Pt_{71}$ nanocubes shows a collective superparamagnetic response with a blocking temperature T_B=80 K at the time scale of the measurement (100 s) and that the individual nanocubes undergo a ferromagnetic-to-paramagnetic phase transition at 250 K. Furthermore, it is demonstrated that from the detailed analysis of the temperature dependent magnetization $M(B)$ loops and field-cooled and/or zero-field-cooled data, the magnitude of the dipolar coupling between the nanocubes can be estimated. Due to the low Curie temperature, the temperature dependence of the magnetization and of the magnetic anisotropy[20] had to be included in the analysis as a correction to the conventional blocking behavior of superparamagnetic ensembles.

The magnetic measurements show three regimes of different magnetic response: (a) Magnetic hysteresis is observed up to a temperature of 75 K; (b) above 75 K, we find a classical superparamagnetic response with no hysteresis; and (c) above 200 K, the magnetization of the individual ferromagnetic nanocubes becomes strongly temperature dependent and vanishes around 250 K. At low temperature [regime (a)], we measure a coercive field B_c=75 mT at 5 K, which monotonically decreases with increasing temperature and vanishes at 75 K (Fig. 4). At the lowest temperature, the ratio of the remanence to saturation magnetization M_{rem}/M_S =0.44 is similar to the theoretically predicted value M_{rem}/M_s=0.5 for an assembly of randomly oriented particles with uniaxial magnetic anisotropy[21] and is much lower than the value M_{rem}/M_s=0.83 expected[22] for particles with a four-fold anisotropy. If one also considers that any magnetic interaction between the particles would slightly increase these theoretical values, we must conclude that the nanocubes exhibit an effective uniaxial anisotropy. This may seem surprising given the cubic shape of the nanocrystals. One should note, however, that only for a crystallographically perfect, unstrained, and compositionally homogeneous $FePt_3$ cube a cubic anisotropy can be expected. Any compositional inhomogeneity at one of the cubes surfaces will contribute an effective uniaxial surface anisotropy per cube. Any deviation from the cubic shape will also result in an effective uniaxial shape anisotropy. As already discussed in the previous section, the shape of the nanocubes is not perfect and also the surface composition may be different at opposite surfaces, resulting in a dominating uniaxial magnetic anisotropy density. A quantitative analysis of the different contributions, i.e., the magnetocrystalline (bulk, surface, edge, and strain) and shape (magnetostatic) anisotropies, is not possible due to the size and shape distributions of the particle ensemble.

Additionally, we find that the magnetization $M(B)$ is not saturated in a field of 5 T and shows a small and constant high-field slope $\Delta M(B)/\Delta B$ at low temperatures. This may be due to the following reasons: (a) the presence of small amounts of paramagnetic phases in the sample due to surfactants and very small magnetic clusters, (b) noncollinearities of the atomic magnetic moments at the cube edges due to magnetic inhomogeneities, (c) antiferromagnetic coupled surface regions of Fe^{+2} and Fe^{+3} ions, and (d) small clusters of fcc Fe. Although we believe that based on our chemical synthesis and our TEM and EDX analyses the presence of a magnetic detectable amount of pure Fe clusters or paramagnetic impurities can be excluded, a clear discrimination of the four possible origins is not possible based on the volumetric magnetization measurement alone.

Above 75 K, the hysteresis vanishes and the magnetic response of the ensemble is reversible, i.e., the $FePt_3$ cubes are expected to be in a superparamagnetic, unblocked state at the time scale of the measurement.[34] Figure 5 shows the

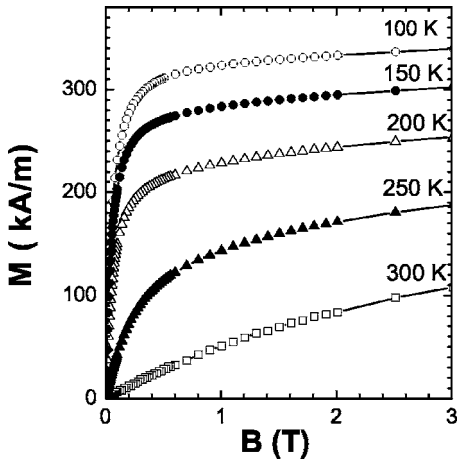

FIG. 5. Magnetization isotherms of the $FePt_3$ nanocubes recorded at different temperatures between 100 and 300 K.

field-dependent magnetization curves $M(B)$ recorded at different temperatures between 100 and 300 K. The magnetization of the sample in fields of up to 5 T decreases and the low-field slope of the curves, i.e., the initial magnetic susceptibility, increases with increasing temperature, as expected from the temperature-dependent behavior of a superparamagnetic ensemble. Due to the volume and the small separation of the nanocubes, the magnetic dipolar interaction cannot be neglected and results in deviations of the magnetization curve from the noninteracting case. For the reduced magnetization of our interacting superparamagnet, we find a scaling law $M/M_S \sim M_S(B/T)$ as suggested by Allia *et al.*[24] in the temperature regime between 100 and 200 K. M_S is the temperature-dependent saturation magnetization recorded at $B=5$ T. Above ~200 K, the changes of the initial susceptibility become even stronger, indicating the approach of the ferromagnetic-to-paramagnetic phase transition within a nanocube at about 255 K.

In order to better understand the magnetization data, the dc susceptibility of the $FePt_3$ assembly was measured between 5 and 370 K in a field of 2 mT after cooling the sample in zero magnetic field [zero-field cooled (ZFC)] and after cooling in a magnetic field of 2 mT [field cooled (FC)]. ZFC and FC susceptibilities [Fig. 6(a)] show the typical behavior for an ensemble of superparamagnetic particles below ~200 K: the FC susceptibility decreases with increasing temperature while the ZFC curve increases and decreases with a maximum at $T \approx 104$ K. At $T \approx 120$ K, the point of irreversibility, the two curves converge and show the same temperature dependence, and the particles are apparently in a superparamagnetic regime which should be characterized by a linear dependence of the inverse susceptibility on the temperature.

The detailed analysis [Fig. 6(b)], however, demonstrates that the inverse initial susceptibility for the $FePt_3$ nanocubes above 120 K does not follow the simple Curie behavior with a constant magnetic moment per particle μ_P. One can clearly distinguish two temperature regimes. Above 250 K, the sample exhibits paramagnetic behavior according to the Curie-Weiss law

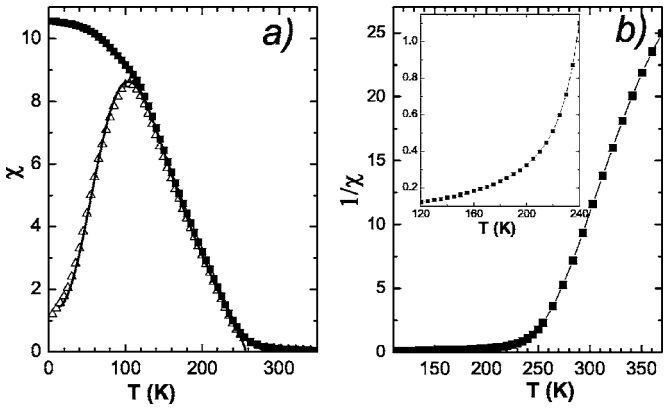

FIG. 6. (a) Temperature dependence of the ZFC (△) and FC (■) susceptibilities of $FePt_3$ nanocubes measured at 2 mT. The symbols represent the experimental values. The solid line is a fit according to Eq. (9) as described in the text. (b) Inverse initial susceptibility $1/\chi$ versus temperature above the blocking temperature. Inset: $1/\chi(T)$ in the superparamagnetic (120–240 K) regime.

$$\chi(T) = \frac{C}{T - T_C}, \tag{2}$$

with the Curie constant $C = n\mu_0\mu^2/3k_B$ and the Curie temperature T_C. μ is an atomic magnetic moment, n is the volume density of the paramagnetic atoms, μ_0 is the permeability of free space, and k_B is the Boltzmann constant. From the slope of $1/\chi$ ($T > 250$ K) in Fig. 6(b), $T_C \sim 255 \pm 5$ K and $C \approx 4.8 \pm 0.02$ K are estimated, indicating the paramagnetic-to-ferromagnetic phase transition of the individual nanocubes at much lower Curie temperature than known for disordered $FePt_3$ bulk samples. Between 120 and 240 K [inset of Fig. 6(b)], the ensemble of $FePt_3$ nanocubes is in a superparamagnetic state with a temperature-dependent magnetic moment μ_p of individual cubes and also a temperature-dependent magnetic dipolar interaction ε_D. In general, the low-field susceptibility of an interacting system in a solid environment can be described by[23,24]

$$\chi(T) = \frac{\eta\mu_0\mu_p^2}{3k_B(T + T^*)}, \tag{3}$$

where η is the number of superparamagnetic moments per unit volume. The temperature T^* is a measure of the effective dipolar interaction energy in an assembly of superparamagnetic particles ε_D (Ref. 24) according to

$$k_B T^* = \varepsilon_D = \frac{\mu_0}{4\pi}\frac{\alpha\mu_p^2}{d^3}, \tag{4}$$

with α being a constant derived from the sum of all dipolar interactions among the particles, and d is an average distance between the neighboring dipoles. For our $FePt_3$ nanocube assembly, the temperature dependences of the particle magnetic moment and of the dipolar interaction [Eq. (3)] have to be taken into account. In the mean-field approximation, the magnetic moment per particle should vary according to

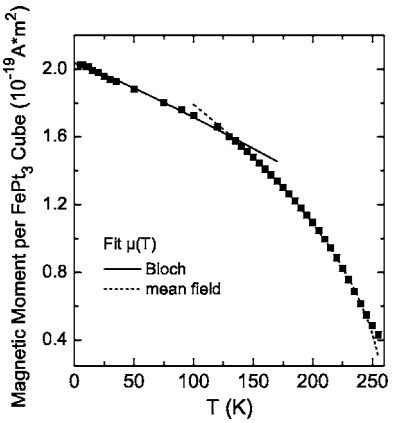

FIG. 7. Temperature dependence of a magnetic moment per $FePt_3$ nanocube. Symbols represent the experimental values determined from the $M(B)$ measurements for temperatures below 120 K and from the ZFC low-field susceptibility above 120 K. The solid line is a fit according to the spin-wave (Bloch) theory [Eq. (7)] and the dashed line represents a fit according to the mean-field theory.

$$\mu_p(T) = \mu_p(0)\left(1 - \frac{T}{T_C}\right)^{1/2}. \tag{5}$$

Combining Eqs. (3) and (5), the inverse initial susceptibility of our nanocube ensemble can be written as

$$\frac{1}{\chi} = \frac{3k_BT_C}{\eta\mu_0\mu_p^2(0)}\frac{T}{(T_C - T)} + \frac{3\alpha}{4\pi\eta d^3}. \tag{6}$$

The solid line in the inset of Fig. 6(b) is the best fit of the experimental data according to Eq. (6). It yields $\alpha \approx 0.35$ and $\mu_p(T=0\ \mathrm{K}) = 2.3\times10^{-19}\ \mathrm{A\,m^2}$. In the fit, we use an average center-to-center distance $d \sim 11$ nm between the neighboring cubes determined from our TEM studies and the Curie temperature $T_C = 255$ K determined from the paramagnetic susceptibility fit. The maximal interaction energy for our particle system is $\varepsilon_D(0) \sim 2.03\times10^{-21}$ J or $\varepsilon_D(0)/k_B = 148.5$ K. The temperature-dependent average magnetic moment per $FePt_3$ cube resulting from this analysis is shown in Fig. 7 together with the low temperature values ($T < 100$ K) which are obtained from the saturation values $M_s(T)/\langle V_p\rangle$ after subtraction of the small high-field slope (Fig. 4).

The thermal decrease of the particle magnetic moment between 5 and 130 K can be fitted to a spin-wave-type dependence as follows:

$$\mu_p(T) = \mu_p(0)(1 - BT^{\beta}), \tag{7}$$

where $\mu_p(0)$, B, and β are the particle magnetic moment at 0 K, the Bloch constant, and the Bloch exponent, respectively. The fit yields $\mu_p(0) \sim 2.03\times10^{-19}\ \mathrm{A\,m^2}$ corresponding to an average magnetic moment per $FePt_3$ formula unit of $\sim 0.63\mu_B$ ($\sim 2.52\mu_B$ per Fe atom when Pt carries no magnetic moment), which is 20% lower than that of the bulk $FePt_3$ alloy. This reduction can be due to partial antiferromagnetic correlations within single nanocubes or the suppression of atomic moments at the surface of the cubes due to oxidation. The Bloch exponent $\beta \sim 1.12$ [bulk $\beta = 1.5$ (Ref. 25)] and the Bloch constant $B \sim 9\times10^{-4}$ are in good agreement with values determined in 5 nm diameter Fe nanoparticles.[26] A linear ($\beta = 1$) decrease of the magnetization of a nanoparticle is expected[27] when the spin-wave energy $E_n = D(n\pi/d)^2 + g\mu_B B_a$ (B_a is the magnetic anisotropy field) of the first excited mode $n=1$ cannot be excited at low temperatures. For our particles with a side length $d=8$ nm and a spin-wave stiffness constant $D = 3.06\pm0.5$ meV nm^2,[28] we calculate $E_1 = 530\ \mu$eV ($B_a = 0.5$ T, $g = 2.09$). Hence, low-energy spin-wave excitations will be possible in the considered temperature interval, yielding an effective $\beta = 1.12$.

Only when using the full temperature dependence of the magnetization (Fig. 7) we can simulate the ZFC behavior of the ensemble [Fig. 6(a)]. In a simplified approach, the position of the peak in the ZFC initial susceptibility T_p is related to the mean blocking temperature $\langle T_B\rangle$ for an ensemble of interacting magnetic particles by[29,30]

$$\langle T_B\rangle = \frac{K_{eff}\langle V_p\rangle + \varepsilon_D}{k_B \ln\left(\frac{t_m}{\tau_0}\right)}, \tag{8}$$

where K_{eff} is the effective magnetic anisotropy energy density, t_m is the observation time that is ~ 100 s for dc superconducting quantum interference device measurements, τ_0 is a microscopic relaxation time of $\sim 10^{-10}$–10^{-11} s. Due to the particle size distribution, the peak temperature T_p is different from the mean blocking temperature $\langle T_B\rangle$. The ratio $\beta = T_p/\langle T_B\rangle$ does not depend on the mean volume of the particle; it depends on the distribution function and its breadth.[31,32] For the lognormal distribution with $\sigma = 0.3$, one calculates $\beta \approx 1.3$ and $\langle T_B\rangle \sim 80$ K for our sample. With this, we can estimate the dipolar interaction $\varepsilon_D(80\ \mathrm{K}) \sim 100$ K and the effective anisotropy $K_{eff} \sim 5.2\times10^4\ \mathrm{J/m^3}$.

In a more refined approach, the temperature dependence of the ZFC curve can be simulated by taking into account the volume distribution $f(V)$ and the temperature dependence of the magnetization, of the dipolar coupling, and of the magnetic anisotropy K_{eff} according to

$$\chi_{ZFC}(T) = \frac{\mu_0 M_s^2(T)}{3[k_BT + \varepsilon_D(T)/\langle V_p\rangle]}\frac{1}{\langle V_p\rangle}\int_0^{V_L(T)} V^2 f(V)dV + \frac{\mu_0 M_s^2(T)}{3[K_{eff}(T) + \varepsilon_D(T)/\langle V_p\rangle]}\frac{1}{\langle V_p\rangle}\int_0^{V_L(T)} Vf(V)dV, \tag{9}$$

where $V_L \equiv [\ln(t_m/\tau_0)]\{k_BT/[K_{eff}(T) + \varepsilon_D(T)/\langle V_p\rangle]\}$ is the volume of the particles at the border of the superparamagnetically fluctuating and the blocked state. The first term describes the susceptibility of the unblocked part of particles, whereas the second term is the susceptibility of the blocked ones.[33,34] The temperature dependence of the magnetic anisotropy can be estimated in the following way. The shape anisotropy is proportional to $M_s^2(T)$ and the magnetocrystalline anisotropy can be calculated according to $K(T) \propto M_s(T)^p$, with $p=10$ for cubic structures and $p=3$ for uniaxial systems. For FePt, $p=2.1$ has been theoretically predicted and experimentally verified.[35] In small particles, the

contribution from the surface anisotropy can be very important, and from thin-film experiments a different temperature dependence is known.[36] This may be the reason why for 6 nm $CoPt_3$ and $FePt_2$ nanoparticle assemblies, a power law $K(T) \propto M_s(T)^6$ was measured,[37,38] whereas for 2.5 nm diameter spherical $Fe_{0.7}Pt_{0.3}$ particles,[34] we found $K(T) \propto M_s(T)^2$. For lack of a better knowledge, we assume $p=2.1$ and obtain the temperature dependence of K_{eff} by using the previously analyzed $M_S(T)$ according to $K_{eff}(T)/K_{eff}(0) = [M_s(T)/M_s(0)]^{2.1}$.

The fit according to Eq. (9) turns out to be very sensitive to the volume distribution, and we find $\sigma=0.5$, which is large in comparison with the geometric value obtained from the TEM analysis. This may be the result of cooperative effects in the interacting particle ensemble, which means that the "magnetic units" are not single particles but particle agglomerates, or clusters, having slightly different sizes. If one also takes into account that the magnetic moment $\mu_p(T) = M_s(T)V_p$ distribution includes the variance in composition, it becomes clear that a larger "volume" distribution has to be used in the fit. An excellent fit [solid line in Fig. 6(a)] is obtained only when the temperature dependence of M_s as discussed above is included. Extrapolating to low temperature, we find the magnetic anisotropy density $K_{eff}=(6.7\pm1)\times10^4$ J/m^3 at 0 K, which is larger than the values known for disordered $FePt_3$ bulk.

IV. CONCLUSION

Single-crystalline chemically disordered $FePt_3$ nanocubes with a side length of ~7.9 nm were synthesized, and the structural and magnetic properties were characterized. We find a ferromagnetic ground state, a 20% reduced magnetic moment per $FePt_3$ formula unit of $\sim0.63\mu_B$, a reduced Curie temperature of 255 K, and an effective magnetic anisotropy energy density $K_{eff}=(6.7\pm1)\times10^4$ J/m^3.

ACKNOWLEDGMENTS

We thank Devendra Chaudhary and H. Zähres for assistance in the TEM measurements and M. Vennemann for the XRD measurements. Financial support by the European Union under Contract No. MRTN-CT-2004-005567 (SyntOrbmag) is acknowledged.

*Present address: Laboratoire de Chimie de Coordination, UPR 8241-CNRS, 205 Route de Narbonne, 31077 Toulouse Cedex 04, France.

†Present address: Unité Mixte de Physique CNRS/THALES, Route départementale 128, 91767 Palaiseau, France.

[1] F. Dumestre, C. Amiens, B. Chaudret, P. Fejes, and P. Renaud, Science **303**, 821 (2004).

[2] N. Shukla, C. Liu, and A. G. Roy, Mater. Lett. **60**, 995 (2006).

[3] M. Chen, J. Kim, J. P. Liu, H. Fan, and S. Sun, J. Am. Chem. Soc. **128**, 7132 (2006).

[4] C. Antoniak *et al.*, Phys. Rev. Lett. **97**, 117201 (2006).

[5] C. Creemers and P. Deurinck, Surf. Interface Anal. **25**, 177 (1997).

[6] P. Beccat, Y. Gauthier, R. Baudoing-Savois, and J. C. Bertolini, Surf. Sci. **238**, 105 (1990).

[7] Rongming Wang *et al.* (unpublished).

[8] O. Dmitrieva, M. Acet, G. Dumpich, J. Kästner, C. Antoniak, M. Farle, and K. Fauth, J. Phys. D **39**, 4741 (2006).

[9] G. E. Bacon and J. Crangle, Proc. R. Soc. London, Ser. A **272**, 387 (1963).

[10] D. Palaith, C. W. Kimball, R. S. Preston, and J. Crangle, Phys. Rev. **178**, 795 (1969).

[11] S. Maat, O. Hellwig, G. Zeltzer, Eric E. Fullerton, G. J. Mankey, M. L. Crow, and J. L. Robertson, Phys. Rev. B **63**, 134426 (2001).

[12] S. Maat, A. J. Kellog, D. Weller, J. E. E. Baglin, and Eric E. Fullerton, J. Magn. Magn. Mater. **265**, 1 (2003).

[13] R. L. Compton, M. J. Pechan, S. Maat, and Eric E. Fullerton, Phys. Rev. B **66**, 054411 (2002).

[14] J. J. M. Franse and R. Gersdorf in *3d, 4d and 5d Elements, Alloys and Compounds*, edited by H. P. J. Wijn, Landolt-Börnstein, Group III Condensed Matter, Vol. 19a (Springer, Berlin, 1996).

[15] S. Sun, C. B. Murray, D. Weller, L. Folks, and A. Moser, Science **287**, 1989 (2000).

[16] Philips Tecnai F20 TEM/STEM/GIF Supertwin microscope with an operating voltage of 200 kV and a point resolution of 0.24 nm. Philips CM12 Twin microscope with LaB6 cathode operating at 120 kV, and a point resolution of 0.35 nm. Both microscopes are equipped with energy dispersive x-ray (EDX) spectroscopy capability.

[17] S. Saita and S. Maenosono, Chem. Mater. **17**, 3705 (2005).

[18] R. Hayn and V. Drchal, Phys. Rev. B **58**, 4341 (1998).

[19] D. Litvinov, J. Appl. Phys. **85**, 2151 (1999).

[20] C. Antoniak, J. Lindner, and M. Farle, Europhys. Lett. **70**, 250 (2005).

[21] E. C. Stoner and E. P. Wohlfarth, Philos. Trans. R. Soc. London, Ser. A **240**, 559 (1948); IEEE Trans. Magn. **27**, 3475 (1991).

[22] M. Walker, P. I. Mayo, K. O'Grady, S. W. Charles, and R. W. Chantrell, J. Phys.: Condens. Matter **5**, 2779 (1993).

[23] K. O'Grady, A. Bradbury, S. W. Charles, S. Menear, and J. Popplewell, J. Magn. Magn. Mater. **31-34**, 958 (1983).

[24] P. Allia, M. Coisson, P. Tiberto, F. Vinai, M. Knobel, M. A. Novak, and W. C. Nunes, Phys. Rev. B **64**, 144420 (2001).

[25] B. D. Cullity, *Introduction to Magnetic Materials* (Addison-Wesley, New York, 1972).

[26] Dajie Zhang, K. J. Klabunde, C. M. Sorensen, and G. C. Hadjipanayis, Phys. Rev. B **58**, 14167 (1998).

[27] S. Mørup and B. R. Hansen, Phys. Rev. B **72**, 024418 (2005).

[28] Value measured for a $Fe_{32}Pt_{68}$ film by spin-wave resonance. C. Antoniak (private communication).

[29] J. L. Dormann, L. Bessais, and D. Fiorani, J. Phys. C **21**, 2015 (1988).

[30] J. L. Dormann and D. Fiorani, J. Magn. Magn. Mater. **140-144**, 415 (1995).

[31] J. S. Jiang and S. Mørup, Nanostruct. Mater. **9**, 375 (1997).

[32] M. F. Hansen and S. Mørup, J. Magn. Magn. Mater. **203**, 214

(1999).
[33] M. Respaud, J. M. Broto, H. Rakoto, A. R. Fert, L. Thomas, B. Barbara, M. Verelst, E. Snoeck, P. Lacante, A. Mosset, J. Osuna, T. O. Ely, C. Amiens, and B. Chaudret, Phys. Rev. B **57**, 2925 (1998).
[34] C. Antoniak, J. Lindner, V. Salgueirino-Maceira, and M. Farle, Phys. Status Solidi A **203**, 2968 (2006).
[35] O. N. Mryasov, U. Nowak, K. Y. Guslienko, and R. W. Chantrell, Europhys. Lett. **69**, 805 (2005).
[36] M. Farle, Rep. Prog. Phys. **61**, 755 (1998).
[37] F. Wiekhorst, E. Shevchenko, H. Weller, and J. Kötzler, Phys. Rev. B **67**, 224416 (2003).
[38] F. Wiekhorst, E. Shevchenko, H. Weller, and J. Kötzler, J. Magn. Magn. Mater. **272**, 1559 (2004).